JOC The Journal of Organic Chemistry

pubs.acs.org/joc Article

Topological Control of Paratropicity via Alternative Ring Fusion in Indacenodithiophene Isomers

Anjana Ranasinghe Meegasmullage, Muhammad Usama Gul Khan, Jacob Mensah, Sean Parkin, Alice E. Bruce, Mitchell R. M. Bruce, Judy I. Wu, and Tomas Marangoni*

Cite This: https://doi.org/10.1021/acs.joc.6c00674 Read Online

ACCESS | Metrics & More | Article Recommendations | Supporting Information

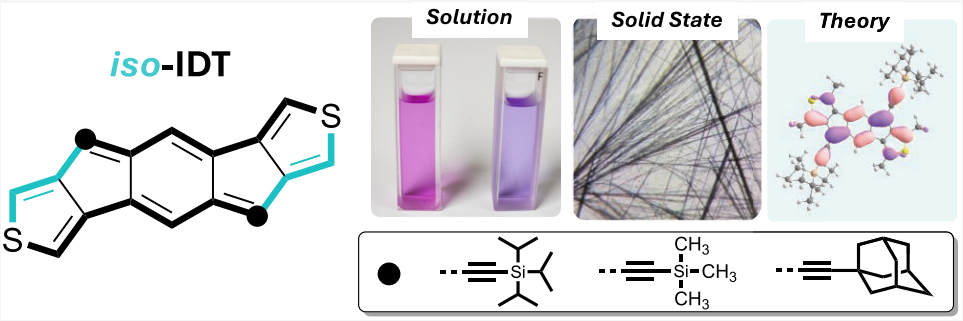

ABSTRACT: We report the synthesis and characterization of a series of isomeric indacenodithiophenes (*iso*-IDTs) bearing various ethynyl substituents at the apical carbons. Absorption spectroscopy, cyclic voltammetry, and density functional theory (DFT) calculations were performed to investigate the electronic properties of these compounds. Notably, analogues with reduced steric protection (i.e., trimethylsilyl, adamantyl) were also successfully isolated and investigated. Computed nucleus-independent chemical shifts and ring current plot analyses reveal that *iso*-IDTs display reduced antiaromatic character compared to indenofluorene (IF) and the previously reported *syn*- and *anti*-fused IDT isomers, suggesting that the π-bond arrangement within the indacenodithiophene π-system can be leveraged for tuning their optoelectronic properties.

INTRODUCTION

Indeno[1,2-*b*]fluorene (IF) and its derivatives have emerged as promising molecular scaffolds for the development of advanced organic materials with potential applications in organic field-effect transistors (OFETs), organic photovoltaics (OPVs), and optoelectronic devices.[1−7] Studies have shown that the electronic and redox properties of IFs can be effectively tuned through π-expansion or substitution of the peripheral benzene rings with heteroarenes,[8−12] as exemplified by many reported examples of pyrrole-, thiophene-, and furan-fused indacenes (Figure 1a).[10,11,13−16] Among the heteroarene-fused indacenes, thiophene-fused systems are the most well-studied and can exhibit distinct electronic properties compared to the benzannelated IFs (e.g., reduced highest occupied molecular orbital (HOMO)−lowest unoccupied molecular orbital (LUMO) energy gaps and enhanced paratropicity).[17−20]

While merging thiophene with the *s*-indacene moiety has led to several indacenodithiophene (IDT) analogues, the main fusion pattern is the one in which the fused thiophene shares its 2 and 3 positions with the *s*-indacene core, resulting in the possible formation of two distinct isomeric families, *syn* or *anti* (Figure 1b).[19,21] This fusion pattern leaves the electronic configuration of the canonically antiaromatic indacene unit ([4*n*] π-electrons) intact while further stabilizing the system by annelation to heteroaromatic subunits.[22] Additionally, it has been shown that the placement of the sulfur atoms along the IDT scaffold perturbs the paratropicity of the π-system; the *syn*-isomer is more antiaromatic than the *anti*-analogue.[23] The observed *syn*- vs *anti*-difference can be rationalized by considering how the position of the heteroatoms affects the charge distribution around the [4*n*] core[21] and by comparing the resonance forms enabled by the *syn*- and *anti*-forms.[24]

Despite recent advances in the development of IDTs, structural modifications that enable systematic tuning of their electronic properties remain limited. Herein, we present the synthesis and characterization of a topologically distinct series of IDTs, which involve fusion of the 3 and 4 positions of the thiophene ring (i.e., *iso*-IDT). The resulting hydrocarbon framework retains the characteristic 5-5-6-5-5 fused ring sequence of *syn*- and *anti*-IDTs but displays alternating double and single bonds along the periphery and sulfur atoms that are

Received: March 23, 2026
Revised: June 29, 2026
Accepted: July 2, 2026

© XXXX The Authors. Published by American Chemical Society

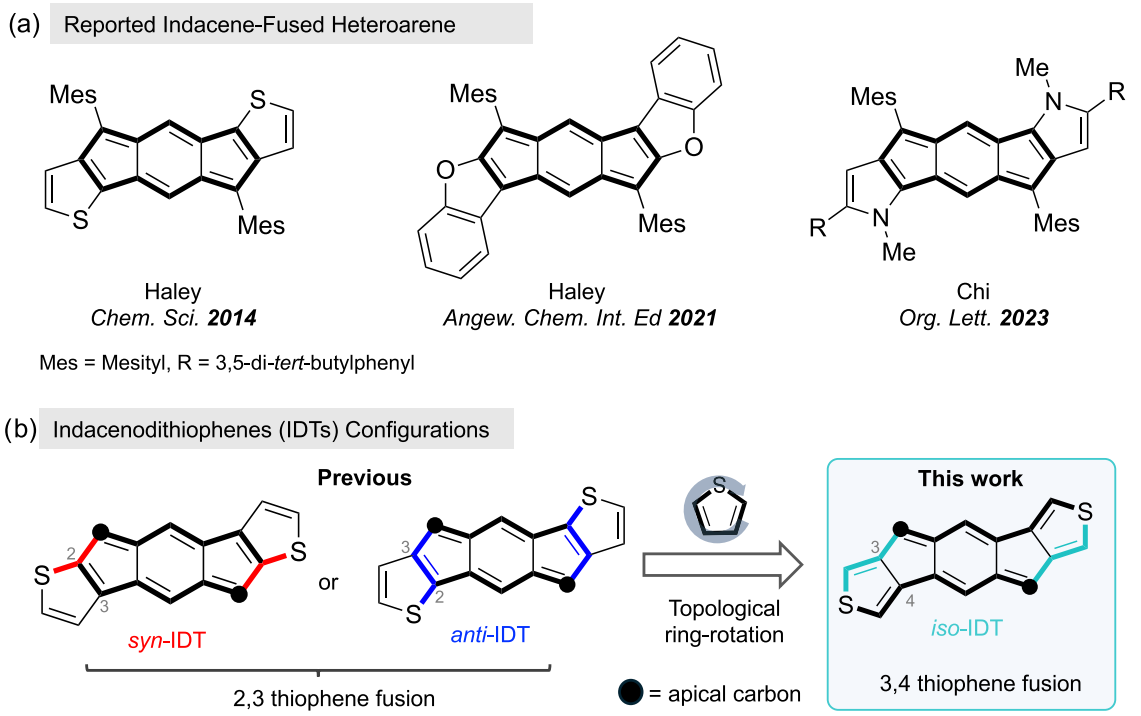

Figure 1. (a) Previously reported heterocycle-fused indacenes featuring a central [4*n*] core (bold). (b) A schematic illustration comparing *syn*- and *anti*-IDTs to *iso*-IDT (this work). Connectivity of the sulfur atoms to the apical carbons is marked in color for *syn*- (red), *anti*- (blue), and *iso*- (cyan).

Scheme 1. Synthesis of *iso*-IDTs 1a–c and Structure of IF Compounds 2a–c (Grey Box)

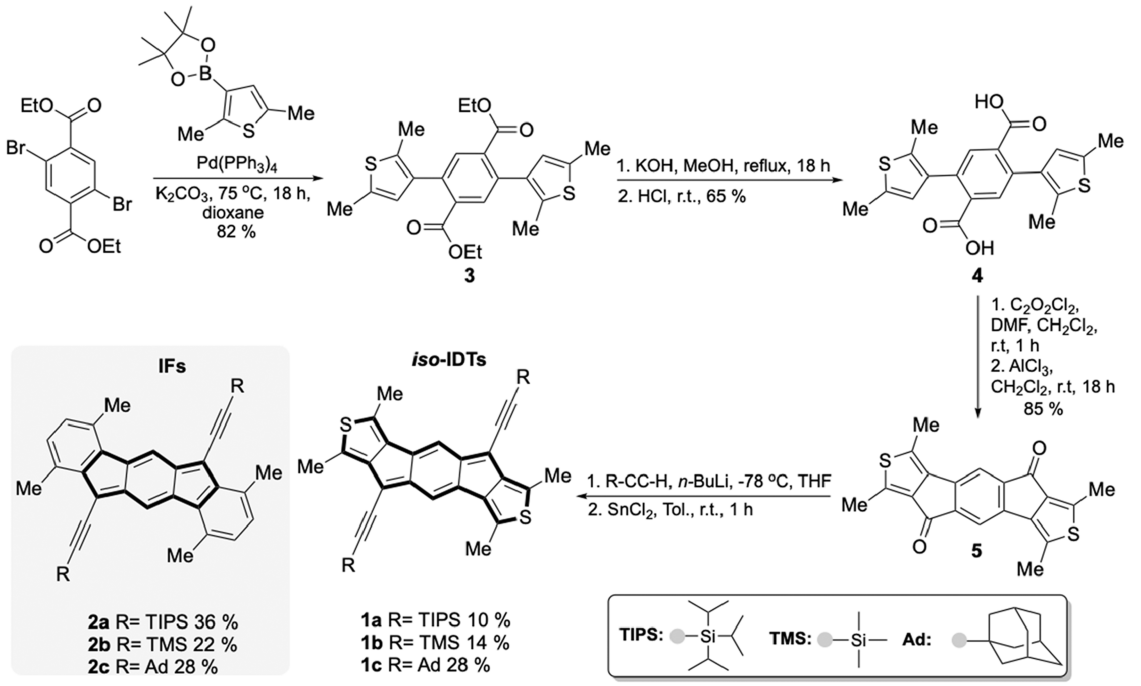

not directly linked to the central [4*n*] core (Figure 1b). This ring topology has not yet been investigated and provides a unique opportunity to increase the understanding of the relationship between π-conjugation patterns and electronic properties in IDT compounds. Through a combination of spectroscopic, electrochemical, and computational studies, we demonstrate that this alternative thiophene fusion pattern can give rise to distinct electronic properties compared to previously reported IDT frameworks, providing insights into the design of functionalized IF systems for the next-generation organic electronic materials.

RESULTS AND DISCUSSION

We prepared the *iso*-IDTs following an "inside-out" approach (Scheme 1) consisting of Suzuki cross-coupling, Friedel–Crafts acylation, and a reductive dearomatization.[25] To

https://doi.org/10.1021/acs.joc.6c00674
J. Org. Chem. XXXX, XXX, XXX−XXX

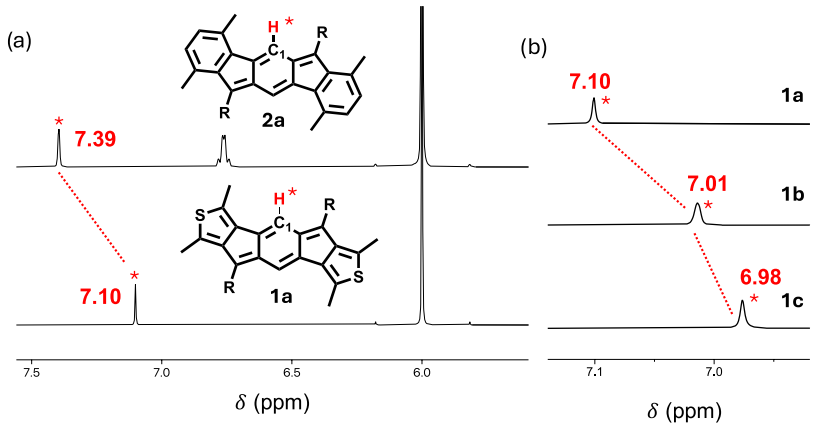

Figure 2. Partial ^{1}H NMR spectra (500 MHz, $C_2D_2Cl_4$, 25 °C) showing the different chemical shift of the central ^{1}H resonance (marked in red) of (a) **1a** and **2a** and (b) **1a**–**c**, illustrating substituent effects at the apical carbons of compounds **1a**–**c**.

selectively obtain the *iso*-IDT core, methyl groups at the 2 and 5 positions of the thiophene precursors were used as blocking groups to prevent undesired isomerization during the Friedel–Crafts acylation step. Three ethynyl substituents with progressively increasing steric protection were placed at the apical carbon, trimethylsilyl- (TMS) ≪ adamantyl- (Ad) < triisopropylsilyl- (TIPS), to investigate the stability of the *iso*-IDT core in solution.[26] Syntheses for **1a**–**c** are reported in Scheme 1. Pd(0)-mediated Suzuki cross-coupling between diethyl 2,5-dibromoterephthalate and 2,5-dimethyl thiophene boronpinacolate produced the intermediate diester **3**, which was subsequently hydrolyzed by treatment with KOH in MeOH to afford the corresponding diacid **4**. Chlorination of the diacid **4** with oxalyl chloride and catalytic dimethylformamide (DMF) followed by treatment with $AlCl_3$ affords diketone **5**. Finally, diketone **5** is subjected to nucleophilic addition with either (triisopropylsilyl)acetylene (TIPSA), trimethylsilylacetylene (TMSA), or 1-ethynyladamantane (Ad-E) in the presence of *n*-BuLi to afford the respective dialcohols, which subsequently undergo reductive dearomatization with $SnCl_2$ to afford the desired compounds **1a**–**c**. For comparison, a set of tetramethylated IF compounds, **2a**–**c**, was also prepared using the same synthetic approach (see Scheme S1 in the SI).

Remarkably, the less sterically shielded TMS derivatives **1b** and **2b** were sufficiently stable to undergo column chromatography and isolation. This differs from previous attempts to generate trimethylsilyl IF derivatives in which dimerization and polymerization occur during the reductive dearomatization step.[27,28] Ethynyladamantane derivatives, **1c** and **2c**, were also isolated and purified by column chromatography. We ascribe the feasibility to isolate these compounds to the relatively mild conditions and short reaction times used during the reductive dearomatization step; the methyl groups also afford some degree of additional steric protection. Nevertheless, the lifetimes of compounds **1b**/**1c** and **2b**/**2c** in solution are relatively short with major decomposition occurring in approximately 24 h in $C_2D_2Cl_4$ at room temperature (see Figure S2 in the SI).

To gain insight into the decomposition of the *iso*-IDT derivatives, samples of **1b** and **1c** were heated at 80 °C for 8 h and subsequently analyzed by gel permeation chromatography (GPC), UV–vis, and NMR spectroscopy (see Figure S3 in the SI). Decomposed mixtures obtained from **1b** and **1c** contained both higher-molecular-weight oligomeric/polymeric species and discrete molecular products. UV–vis spectroscopy of the decomposed samples revealed blue-shifted absorption profiles and a disappearance of the low-energy electronic transitions relative to **1b** and **1c** (*vide infra*), supporting a decomposition mechanism involving intermolecular coupling. The identity of the decomposition products could not be unambiguously established due to the complexity of the mixtures obtained and the poor ionization efficiency of the *iso*-IDT derivatives in mass spectrometry analyses.

^{1}H NMR analyses were performed to characterize the paratropicity of the *iso*-IDTs. The signals corresponding to the protons on the central 6-membered rings of **1a**–**1c** and **2a** are shown in Figure 2 (see H marked in red). Notably, the proton resonance for *iso*-IDT **1a** (7.10 ppm) exhibits a pronounced upfield shift compared to **2a** (7.39 ppm) but is shifted downfield relative to previously reported *syn*- and *anti*-IDT analogues (ca. 6.1 ppm).[19] Therefore, the *iso*-IDTs may be considered to exhibit more diene-like character. ^{1}H NMR signals for the corresponding protons in **1a** (7.10 ppm), **1b** (7.01 ppm), and **1c** (6.98 ppm) were progressively shifted upfield, although the values remain relatively close due to the similar electron donating capability of TIPS, TMS, and Ad (Figure 2b). ^{13}C distortionless enhancement by polarization transfer (^{13}C-DEPT) NMR spectroscopy experiments were performed for **1a**–**1c** to quantify the effects of the ethynyl substituents on the carbon framework. ^{13}C-DEPT NMR results revealed similar chemical shift values for carbon atom C_1 (Figure S4 of the SI), suggesting that the electronic structures for **1a**–**1c** are comparable. Accordingly, the computed carbon chemical shifts at UB97-2/6-311+G(d,p)//UωB97XD/def2-SVP for C_1 in **1a** (116.9 ppm), **1b** (116.9 ppm), and **1c** (116.4 ppm) are all close.

Electronic effects of the ethynyl TIPS, TMS, and Ad substituents were also investigated by infrared (IR) spectroscopy (Figure S5 in the SI). Compounds **1a** and **1b** exhibited medium-intensity C ≡ C stretching bands at 2120 and 2116 cm^{-1}, respectively, which agree with a more polarizable silicon-containing substituent. In contrast, compound **1c** displayed a weaker alkyne stretching band at 2195 cm^{-1}, which agrees with the nonpolar nature of the carbon-disubstituted alkyne. Computed asymmetric C≡C stretching frequencies for **1a** (2233.9 cm^{-1}), **1b** (2233.7 cm^{-1}), and **1c** (2313 cm^{-1}) show the same trends.

Electronic absorption spectra for **1a**–**1c**, **2a**, and **5** are shown in Figure 3a (cf. **2a**–**2c** and **8** in Figure S6). Spectra for

https://doi.org/10.1021/acs.joc.6c00674
J. Org. Chem. XXXX, XXX, XXX–XXX

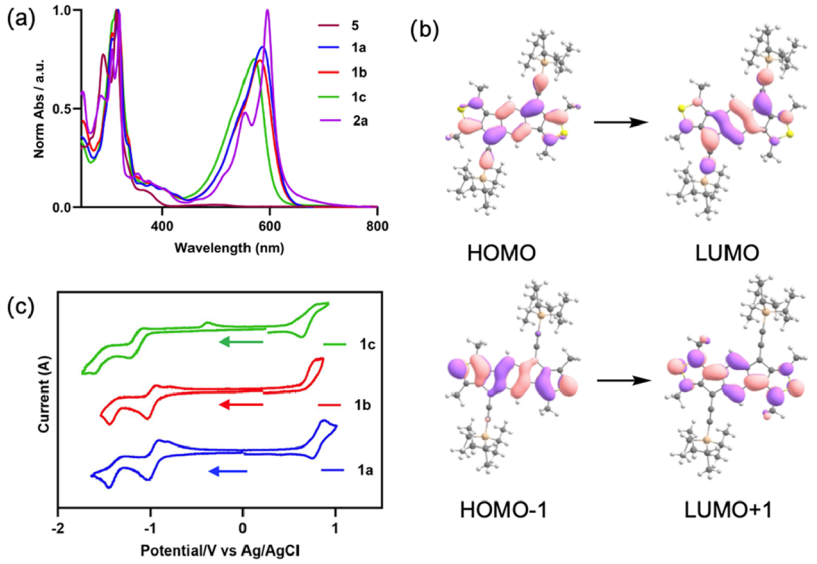

Figure 3. (a) Absorption spectrum of *iso*-IDT derivatives **1a−c**, diketone **5** and IF **2a** (CH_2Cl_2, 25 °C). (b) Orbitals involved in the major electronic transitions (HOMO → LUMO and HOMO − 1 → LUMO + 1) of **1a** computed at ωB97XD/def2-SVP. (c) Cyclic voltammetry (CV) of **1a−c** (following IUPAC convention, the arrows indicate the direction of the scan).

the diketones (**5** and **8**) display intense absorptions from approximately 260 to 360 nm with low intensity broad absorption bands appearing in the 430−560 nm range. Spectra for the *iso*-IDT (**1a−1c**) and IF (**2a−2c**) derivatives are red-shifted relative to their parent diketones (**5** and **8**) as a consequence of extended π-conjugation. Compounds **1a−c** show high absorbance bands from 270 to 370 nm and broadened lower energy bands in the range of 450−650 nm (Figure 3a). In contrast, **2a−c** show high absorbance bands ranging from 290 to 340 nm and sharper absorption bands in the region between 470 and 650 nm which are slightly red-shifted (Figure S6). The broadened lower energy bands of **1a−c** are consistent with the behavior previously reported for *syn*- and *anti*-IDT derivatives and are characteristic of thiophene-fused indacene systems.[19] Time-dependent density functional theory (TD-DFT) calculations at the ωB97XD/def2-SVP level reveal two major transitions for **1a**, at 265.4 nm (HOMO − 1 to LUMO + 1) and 596.4 nm (HOMO to LUMO), and two for **2a**, at 267.6 nm (HOMO − 1 to LUMO + 1) and 622.6 nm (HOMO to LUMO) (see Figures 3b and S14 in the SI). Concentration-dependent UV−vis measurements of **1a** revealed no change in the absorption profiles (Figure S7 in the SI), suggesting the absence of aggregation under the conditions examined. Trends across the ethynyl TIPS-, TMS-, and Ad-substituted IF and *iso*-IDT derivatives parallel each other: the TIPS derivatives are the most red-shifted (λ_{max} = 586 nm for **1a** and 596 nm for **2a**), followed by the TMS derivatives (λ_{max} = 582 nm for **1b** and 592 nm for **2b**) and the Ad derivatives (λ_{max} = 572 nm for **1c** and 586 nm for **2c**).

The photophysical and electrochemical properties of *iso*-IDTs were investigated in CH_2Cl_2 solution, and the main features are summarized in Table 1. The electrochemical properties of IDTs **1a−1c** (Figure 3c) and S8IFs **2a−2c** (Figures S9) were investigated by cyclic voltammetry (CV). Compounds **1a−1c** and **2a−2c** undergo a reversible reduction to the radical anion form (A/A^-), followed by an irreversible reduction to the dianion. Oxidation processes for both series of compounds are irreversible, although some quasi-reversible behavior is noted for **1a** and **2a**. The reduction potentials for

Table 1. Electrochemical and Optical Data for *iso*-IDT 1a−c and IFs 2a−c

	electrochemical[a]					optical	
compound	$E_{p(ox)}$ (A^+/A)	$E_{p(red)}$ (A/A^-)	E_{HOMO}	E_{LUMO}	E_{gap}	λ_{max} (nm)	E_{opt}
1a	0.88	−1.05	−5.68	−3.75	1.93	586	1.96
2a	1.23	−0.62	−6.03	−4.18	1.86	596	2.00
1b	0.77	−1.04	−5.57	−3.76	1.81	582	1.97
2b	1.09	−0.79	−5.89	−4.01	1.88	592	2.01
1c	0.79	−1.24	−5.59	−3.56	2.03	572	2.04
2c	0.90	−0.92	−5.70	−3.88	1.82	586	2.03

[a]Electrochemical potentials are in volts and energies in electronvolts. E_{HOMO} and E_{LUMO} were estimated assuming an ionization energy of 4.8 eV for ferrocene.

1a−1c are more negative than those for **2a−2c** (see Table 1). Peak potentials for the first reduction (A/A^-) and oxidation (A^+/A) processes were used to estimate the energies of the HOMO and LUMO, respectively. The electrochemical HOMO−LUMO gaps (E_{gap}) for **1a** vs **2a** and **1b** vs **2b** are similar, differing only by 0.07 eV, while that for **1c** vs **2c** differs by 0.21 eV. We note that the E_{gap} values for **1a** (1.93 eV), **1b** (1.81 eV), and **1c** (2.03 eV) are comparable to those previously reported for aryl-substituted *anti*- and *syn*-IDTs (1.85−1.88 eV),[19] suggesting that changing the thiophene unit from a 2,3- to 3,4-fusion topology does not largely affect the electrochemical properties of IDTs. The trends for E_{gap} and E_{opt} do not necessarily follow each other, since the former depends also on the relative stabilization of the oxidized and reduced states. As shown in Table 1, the optical gap (E_{opt}) of **1a** (1.96 eV) is narrower than that of **2a** (2.00 eV), which is consistent with a more upfield shifted ^{1}H NMR signal for **1a**. The E_{opt} for **1b** (1.97 eV) is also narrower than that for **2b** (2.01 eV), while those for **1c** (2.04 eV) vs **2c** (2.03 eV) are nearly equal.

Single crystals suitable for X-ray diffraction of compounds **1a**, **2a**, and diketones **5** and **8** were grown by vapor diffusion of acetonitrile into CH_2Cl_2. For **1a**, two polymorphs were

https://doi.org/10.1021/acs.joc.6c00674
J. Org. Chem. XXXX, XXX, XXX−XXX

obtained: one monoclinic (here designated $\mathbf{1a_1}$) and one triclinic ($\mathbf{1a_2}$). Molecular ellipsoid plots (50% probability) of $\mathbf{1a_1}$ and **2a** are displayed in Figures 4a,b and S10. Structures of the precursor diketones (**5** and **8**) are provided in the SI (Figures S11 and S12). All of the crystals obtained were centrosymmetric.

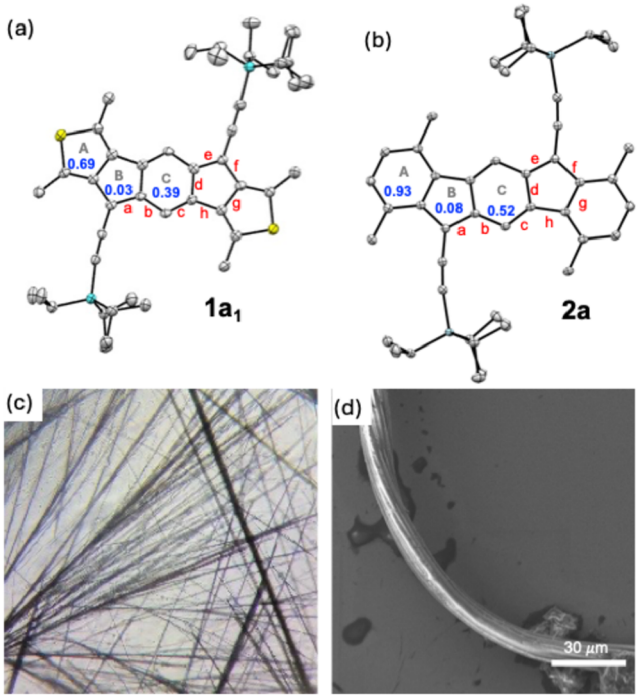

Figure 4. Ellipsoid plot of (a) $\mathbf{1a_1}$ and (b) **2a** with thermal ellipsoids drawn at the 50% probability level (gray = carbon, yellow = sulfur, and cyan = silicon); selected bond types are displayed in red, HOMA (harmonic oscillator model of aromaticity) values in blue, and ring type in gray. Optical microscopy (c) (10×) and scanning electron microscopy (SEM) images (d) of the fiber-like crystals obtained by the vapor diffusion of **1a** in CH_2Cl_2−acetonitrile.

Both polymorphs of **1a** and **2a** display a planar core with no apparent structural distortion on the central ring system despite the neighboring presence of the methyl and TIPS groups. However, the ethynyl C≡C−Si angle deviates from linearity by approximatively 2° for **1a** and 12° for **2a**. Bond length analyses of the central core (Table 2) showed that both molecules displayed similar *para*-quinoidal features for the central tricyclic unit. In both structures, the a, c, and e bond lengths range from 1.357 to 1.401 Å, suggesting double bond character, while the d and f bond lengths range from 1.45 to 1.464 Å, suggesting single bond character. Minor differences in bond lengths are observed between $\mathbf{1a_1}$ and **2a** at bond g, which corresponds to the fused bond between the indacene core and aromatic subunit (i.e., thiophene in $\mathbf{1a_1}$ and benzene in **2a**). *iso*-IDT derivative $\mathbf{1a_1}$ shows a slightly longer g bond (1.437 Å) than **2a** (1.422 Å). We note that the fused bond g in $\mathbf{1a_1}$ is higher compared to all of the previously reported thiophene-fused indacenes (e.g., 1.389 Å for *anti*-IDT, 1.385 Å for *syn*-IDT, and 1.396 Å for ethynyl TIPS functionalized indacenedibenzothiophenes, IDBTs), in which the sulfur atoms are directly bonded to the indacene core.[19,29] Using the bond length obtained from the X-ray structures of $\mathbf{1a_1}$ and **2a**, HOMA (harmonic oscillator model of aromaticity) values were calculated for each ring (Figure 4a,4b, in blue).[30,31] Consistent with computational (*vide infra*) and NMR analyses, HOMA indicates a higher level of bond length alternation (BLA) for the central rings of **1a** compared to **2a**. HOMA values for ring C of **1a** (0.39) is lower than that of **2a** (0.52) indicating decreased π-delocalization and a more diene-like indacene core in **1a**.

Table 2. Selected Bond Length a−h for Compounds $\mathbf{1a_1}$ and 2a

bonds	$\mathbf{1a_1}$ (Å)	2a (Å)
a	1.401(4)	1.394(13)
b	1.417(4)	1.423(13)
c	1.357(4)	1.368(13)
d	1.458(4)	1.45(13)
e	1.400(4)	1.394(13)
f	1.463(4)	1.464(13)
g	1.437(4)	1.422(13)
h	1.470(4)	1.471(13)

Optical and scanning electron microscopy (SEM) analyses reveal that **1a** assembles into long and flexible tape-like crystals resembling microfibers under both vapor diffusion and simple evaporation conditions (Figure 4c,d). Dimensions of the tape-like crystals ranged from 1 to 10 μm in thickness and several mm in length. Upon simple evaporation from CH_2Cl_2 solutions, the formation of the microfibers was extremely rapid and could be observed in seconds under an optical microscope (see Figure S13 in the SI). Since molecular packing in the solid state largely impacts the electronic and physical properties of organic semiconductor materials, we investigated the crystal packing of $\mathbf{1a_1}$, $\mathbf{1a_2}$, and **2a** (Figure 5). In $\mathbf{1a_1}$, the molecules are π−π-stacked with overlapping adjacent thiophene rings to form extended multiply stacked chains. In **2a**, the molecules feature parallel slip-stacked chains formed by π−π overlap of the benzene rings.

To better understand the interactions between *iso*-IDTs in solution, DFT calculations of a dimer model, in which the relative slip stacked positions of the **1a** were fixed based on the crystal structure of **1a**, were performed (Figure S15). A constrained energy scan by varying the stacking distance (r) revealed a relatively large interaction energy (~12 kcal/mol) at a ca. 3.5 Å equilibrium intermolecular distance which can be ascribed to dispersion interactions originating between the isolated molecules of **1a**.[28]

Computed nucleus-independent chemical shifts, $NICS(1)_{zz}$[32,33] and NICS2BC[34] plots at the (U)B97-2/6-311+G(d,p)//(U)ωB97X-D/def2-SVP level suggest that *iso*-IDT exhibits substantially weakened paratropicity compared to IF as well as *syn*- and *anti*-IDT (Figure 6).[19] We attribute this difference to an expanded [4*n*] π-conjugation pathway in *iso*-IDT, which features alternating single and double bonds along the molecular perimeter. Notably, the fused bond between the aromatic rings and the *s*-indacene core is longer in *iso*-IDT (1.441 Å), relative to IF (1.417 Å), *syn*-IDT (1.393 Å), and *anti*-IDT (1.389 Å) (Figure 6, bonds in lilac color). These trends are consistent with the inverse correlation previously reported by Haley et al., in which increased paratropicity at the [4*n*] core is associated with shorter fused bonds connecting the [4*n*] core to the annelated aromatic rings.[22] Computed $NICS(1)_{zz}$ values for the substituted derivatives follow the same trend and are provided in Figure S16.

https://doi.org/10.1021/acs.joc.6c00674
J. Org. Chem. XXXX, XXX, XXX−XXX

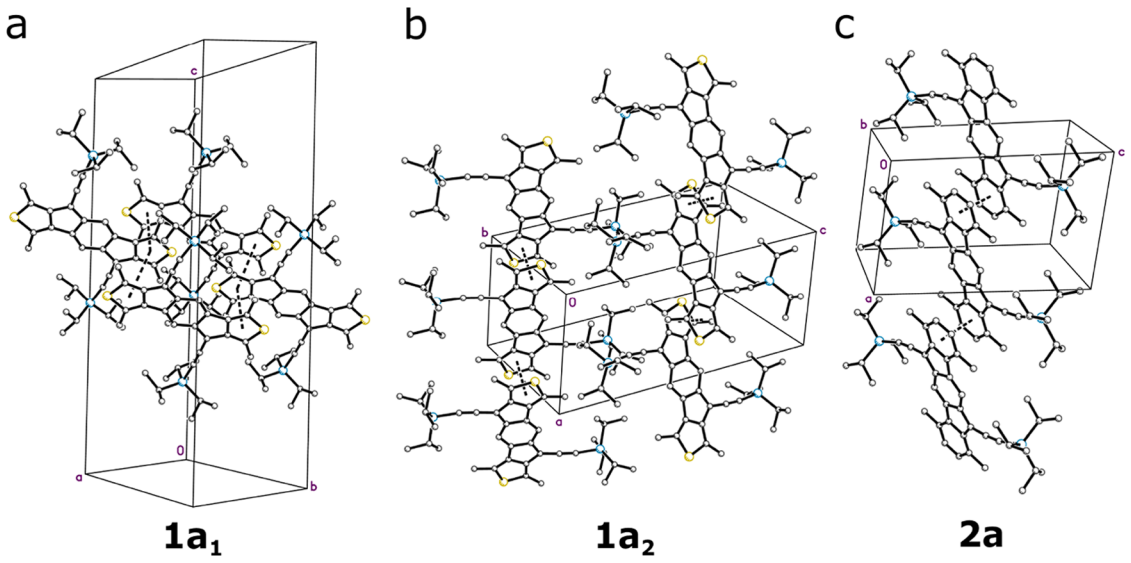

Figure 5. Partial packing plots of (a) $\mathbf{1a_1}$, (b) $\mathbf{1a_2}$, and (c) **2a**. Stacking of molecules by $\pi-\pi$ interactions is shown as solid dashed lines. Hydrogen atoms are omitted to improve clarity.

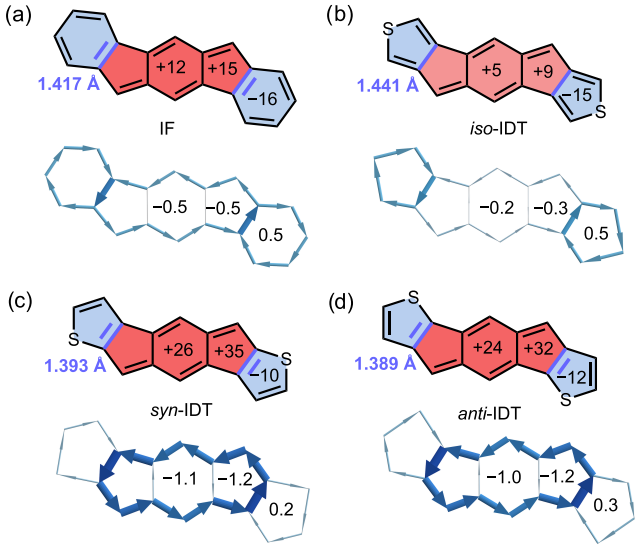

Figure 6. Computed NICS(1)$_{zz}$ values at each of the ring centers and NICS2BC bond currents and ring current plots for (a) IF, (b) *iso*-IDTs, (c) *syn*-IDT, and (d) *anti*-IDT. Calculated fused bond lengths between the *s*-indacene core and aromatic subunits are highlighted in lilac. All calculations were performed at (U)B97-2/6-311+G(d,p)//(U)ωB97X-D/def2-SVP.

CONCLUSIONS

In summary, a series of isomeric indacenodithiophenes, or *iso*-IDTs, featuring the fusion of a thiophene subunit at the 3 and 4 positions has been synthesized and characterized. The *iso*-IDTs exhibit optical, magnetic, and electrochemical properties that are distinct from those of the previously reported *syn*- and *anti*-IDTs as well as the structurally analogous IFs. The *iso*-IDTs feature alternating single and double bonds around the periphery of the π-system and are more "diene-like" compared to the *syn*- and *anti*-IDTs. These findings provide insights for understanding the relationship between double bond topologies and the electronic structures of polycyclic antiaromatic hydrocarbons.

EXPERIMENTAL PART

General Information

All solvents and reagents were obtained from commercial sources and used as received. Air-sensitive reactions were carried out under an inert atmosphere (N_2) using a Schlenk line. Purifications were performed by using column chromatography packed with silica gel 60 from Millipore (0.063−0.200 mm, mesh). ^{1}H and ^{13}C NMR spectra were recorded at room temperature (unless specified) on a Bruker Avance Neo 500 MHz (^{1}H: 500 MHz, ^{13}C: 125 MHz) spectrometer, by using $CDCl_3$, $C_2D_2Cl_4$, CD_2Cl_2, or dimethyl sulfoxide-d_6 (DMSO-d_6) as solvents. The following abbreviations were used to explain the multiplicities: s = singlet, d = doublet, dd = doublet of doublet, st = triplet, q = quartetm = multiplet, br = broad. Cyclic voltammetry was performed using a Princeton Applied Research, Model 273 potentiostat with a conventional three-electrode cell at room temperature under a nitrogen atmosphere with a glassy carbon (3 mm diameter) working electrode, Pt wire counter electrode, and Ag/$AgNO_3$ reference electrode. The glassy carbon electrode was polished with 1.0 μm monocrystalline diamond suspension using a figure-eight motion. The electrolyte solution (0.1 M) was prepared from CH_2Cl_2 and tetra-*n*-butylammonium triflate (Bu_4NOTf). The CH_2Cl_2 was degassed by nitrogen gas sparging for 10 min prior to the measurements. Ferrocene was added as an internal reference, and potentials were adjusted to the Cp_2Fe^+/Cp_2Fe couple at $E_{1/2}$ = 0.46 V vs saturated calomel electrode (SCE). Potentials are the averages of three or more scans at 50 mV/s recorded during cyclic voltammetry (CV) experiments for each compound at concentrations between 1.5 and 3 mM in 0.1 M Bu_4NOTf in CH_2Cl_2 at a glassy carbon working electrode with a Pt counter electrode and $Ag/AgNO_3$ reference. Ferrocene was used as an internal reference ($E_{1/2}$ = 0.46 V vs SCE for Cp_2Fe^+/Cp_2Fe). Electrochemical potentials are in V and energies in eV. The energies of the HOMO and LUMO (E_{HOMO} and E_{LUMO}) were estimated assuming an ionization energy of 4.8 eV for ferrocene. Ultraviolet−visible (UV−vis) absorption spectra were recorded using an Agilent Cary 60 spectrophotometer in CH_2Cl_2 at room temperature. ESI High-Resolution Mass Spectra (HR-MS) were acquired on a Waters Synapt G2-Si ESI/LC-MS spectrometer, EI HR-MS on a Water GCT Premier EI/CI/FD/FI, and MALDI-TOF HR-MS on a Bruker neofleX Matrix-Assisted Laser Desorption Ionization coupled with a tandem Time-of-Flight mass spectrometer (MALDI-TOF/TOF MS).

Compound 3. In a flame-dried Schlenk tube, 1,4-dioxane (40 mL), 1 M K_2CO_3 (40 mL), diethyl 2,5-dibromoterephthalate (1.0 g, 2.63 mmol), and 2-(2,5-dimethylthiophen-3-yl)-4,4,5,5-tetramethyl-

https://doi.org/10.1021/acs.joc.6c00674
J. Org. Chem. XXXX, XXX, XXX−XXX

1,3,2-dioxaborolane (1.57 g, 6.59 mmol) were mixed under a N_2 atmosphere. The mixture was then degassed by the freeze−pump−thaw method twice, and $Pd(PPh_3)_4$ (0.15 g, 0.13 mmol) was added. The resulting solution was degassed one last time and then stirred for 18 h at 75 °C, in an oil bath, under a N_2 atmosphere. The reaction was then cooled to room temperature and extracted with CH_2Cl_2 and DI water. The organic layer was dried over $MgSO_4$, filtered, and evaporated to dryness. The crude product was purified by column chromatography (SiO_2, 7:3 hexane/CH_2Cl_2) affording compound **3** (0.96 g, 82%) as a pale-yellow solid. ^{1}H NMR (500 MHz, $CDCl_3$): δ 7.73 (s, 2H), 6.55 (s, 2H), 4.17 (q, J = 7.1 Hz, 4H), 2.44 (s, 6H), 2.23 (s, 6H), 1.13 (t, J = 7.1 Hz, 6H). $^{13}C\{^1H\}$ NMR (125 MHz, $CDCl_3$): δ 167.7, 136.4, 136.2, 135.4, 134.2, 132.8, 132.5, 127.4, 61.4, 15.3, 14.0, 13.7; ESI HR-MS: calculated for $C_{24}H_{26}O_4S_2Na$ $[M + Na]^+$ 465.1170, found 465.1164.

Compound 4. In a round-bottom flask equipped with a reflux condenser and stirring bar, a mixture of **3** (0.96 g, 2.17 mmol), methanol (100 mL), and 1 M KOH (100 mL) was stirred at reflux overnight, using a heating mantle, under a N_2 atmosphere. After cooling, the methanol was removed by rotary evaporation and concentrated HCl was added dropwise to the resulting aqueous solution until no more precipitation occurred. The resulting precipitate was filtered and washed with H_2O and vacuum-dried at 60 °C to obtain compound **4** (0.54 g, 65%) as a white solid. ^{1}H NMR (500 MHz, DMSO-d_6): δ 13.00 (s, 2H), 7.57 (s, 2H), 6.64 (s, 2H), 2.39 (s, 6H), 2.20 (s, 6H). $^{13}C\{^1H\}$ NMR (125 MHz, DMSO-d_6): δ 168.4, 136.1, 134.7, 134.5, 134.4, 132.0, 131.4, 127.5, 14.8, 13.5; ESI HR-MS: calculated for $C_{20}H_{17}O_4S_2$ $[M - H]^-$ 385.0568, found 385.0562.

Compound 5. In a flame-dried Schlenk tube, oxalyl chloride (0.46 mL, 5.44 mmol) was added to a solution of **4** (0.52 g, 1.35 mmol) in anhydrous CH_2Cl_2 (35 mL) under a N_2 atmosphere. To this mixture, anhydrous DMF (0.21 mL, 2.71 mmol) was added dropwise at room temperature, and the reaction mixture was stirred under a N_2 atmosphere for 1 h. The resulting solution was evaporated to dryness, redissolved in anhydrous CH_2Cl_2 (45 mL) under a N_2 atmosphere, and cooled to 0 °C and then $AlCl_3$ (0.85 g, 6.38 mmol) was added. The mixture was stirred for 18 h at room temperature under a N_2 atmosphere. The reaction mixture was poured into ice-cold pH = 1 HCl solution (100 mL), and the obtained orange precipitate was filtered, washed with H_2O, and vacuum-dried at 60 °C to yield compound **5** (0.40 g, 85%) as an orange solid. ^{1}H NMR (500 MHz, $C_2D_2Cl_4$, 30 °C): δ 7.65 (s, 2H), 2.62 (s, 6H), 2.55 (s, 6H). $^{13}C\{^1H\}$ NMR (125 MHz, $C_2D_2Cl_4$, 80 °C): δ 185.3, 145.9, 144.9, 140.4, 139.2, 137.7, 130.2, 116.8, 13.4, 13.3; EI HR-MS: calculated for $C_{20}H_{14}O_2S_2$ $[M]^+$ 350.0435, found 350.0428.

Compound 1a. In a flame-dried Schlenk tube, (triisopropylsilyl)-acetylene (TIPSA) (0.32 g, 1.77 mmol) was dissolved in dry tetrahydrofuran (THF) (33 mL) and the solution was cooled to −78 °C. To the resulting mixture, 1.6 M *n*-BuLi (1 mL, 1.6 mmol) was added, and all was stirred at −78 °C for 1 h under a N_2 atmosphere. Compound **5** (0.20 g, 0.57 mmol) was then added, and the reaction mixture was stirred overnight at room temperature under a N_2 atmosphere. The resulting solution was quenched with 1 M NH_4Cl (20 mL) and then extracted with CH_2Cl_2. The organic layer was dried over $MgSO_4$, filtered, and evaporated to dryness. The crude diol was redissolved in anhydrous toluene (32 mL) under N_2 and transferred to a flame-dried Schlenk tube. Anhydrous $SnCl_2$ (0.43 g, 2.27 mmol) was then added to the solution, and the reaction mixture immediately turned purple. The reaction was monitored via TLC, and after 1 h, the reaction mixture was filtered through a short silica column (eluent: hexane) to afford the crude compound, which was further purified by column chromatography (SiO_2, solvent: hexane) to give **1a** (0.04 g, 10%) as a dark purple solid. ^{1}H NMR (500 MHz, $C_2D_2Cl_4$): δ 7.10 (s, 2H), 2.56 (s, 6H), 2.46 (s, 6H), 1.17 (m, 42H). $^{13}C\{^1H\}$ NMR (125 MHz, $CDCl_3$): δ 148.5, 142.8, 136.6, 134.2, 129.8, 129.0, 116.9, 116.1, 106.8, 103.1, 18.9, 13.6, 12.8, 11.5; EI HR-MS: calculated for $C_{42}H_{56}S_2Si_2$ $[M]^+$ 680.3362, found 680.3376.

Compound 1b. In a flame-dried Schlenk tube, trimethylsilylacetylene (TMSA) (0.28 g, 2.85 mmol) was dissolved in dry THF (20 mL) and the solution was cooled to −78 °C. To the resulting solution, 1.6 M *n*-BuLi (1.68 mL, 2.69 mmol) was added, and the mixture was stirred at −78 °C for 1 h under a N_2 atmosphere. Compound **5** (0.1 g, 0.29 mmol) was then added, and the reaction mixture was stirred overnight at room temperature under a N_2 atmosphere. The reaction mixture was quenched with 1 M NH_4Cl (20 mL) and was extracted with CH_2Cl_2. The organic layer was dried over $MgSO_4$, filtered, and evaporated to dryness. The crude diol was redissolved in anhydrous toluene (20 mL) under N_2 and transferred to a flame-dried Schlenk tube. Anhydrous $SnCl_2$ (0.22 g, 1.14 mmol) was added, and the reaction mixture immediately turned purple. The reaction was monitored via TLC, and after 1 h, the reaction mixture was filtered through a short silica column (eluent: hexane) to afford the crude compound, which was further purified by column chromatography (SiO_2, solvent: hexane/CH_2Cl_2 9:1) to give **1b** (0.021 g, 14%) as a dark purple solid. ^{1}H NMR (500 MHz, $CDCl_3$) δ 7.01 (s, 2H), 2.52 (s, 6H), 2.49 (s, 6H), 0.29 (s, 18H). $^{13}C\{^1H\}$ NMR (125 MHz, CD_2Cl_2): δ 147.9, 143.1, 136.7, 134.7, 130.8, 129.9, 117.1, 116.3, 111.0, 101.5, 14.1, 12.8, 0.1; ESI HR-MS: calculated for $C_{30}H_{32}S_2Si_2$ $[M]^+$ 512.1484, found 512.1490.

Compound 1c. In a flame-dried Schlenk tube, 1-ethynyladamantane (0.19 g, 1.17 mmol) was dissolved in dry THF (20 mL) and the solution was cooled to −78 °C. 1.6 M *n*-BuLi (0.72 mL, 1.15 mmol) was added, and the mixture was stirred at −78 °C for 1 h, under N_2 atmosphere. Compound **5** (0.10 g, 0.29 mmol) was then added, and the reaction mixture was stirred overnight at room temperature under a N_2 atmosphere. The reaction mixture was quenched with 1 M NH_4Cl (20 mL) and was extracted with CH_2Cl_2. The organic layer was dried over $MgSO_4$, filtered, and evaporated to dryness. The crude diol was redissolved in anhydrous toluene (20 mL) under N_2 and transferred to a flame-dried Schlenk tube. Anhydrous $SnCl_2$ (0.22 g, 1.16 mmol) was added to the reaction mixture, and the reaction mixture immediately turned purple. The reaction was monitored via TLC, and after 1 h, the reaction mixture was filtered through a short silica column (eluent: hexane) to afford the crude compound, which was further purified by column chromatography (SiO_2, solvent: hexane/CH_2Cl_2 9:2) **1c** (0.05 g, 28%) as a dark purple solid. ^{1}H NMR (500 MHz, $C_2D_2Cl_4$) δ 6.98 (s, 2H), 2.55 (s, 6H), 2.52 (s, 6H), 2.02 (br, 18H), 1.75 (br, 12H). $^{13}C\{^1H\}$ NMR (125 MHz, $C_2D_2Cl_4$) δ 145.8, 143.0, 136.3, 133.4, 129.2, 128.0, 120.2, 116.8, 115.3, 113.3, 42.6, 36.2, 31.0, 27.8, 13.7, 12.5; MALDI-TOF HR-MS: calculated for $C_{44}H_{44}S_2$ $[M]^+$ 636.2884, found 636.2864.

■ ASSOCIATED CONTENT

Data Availability Statement

The data underlying this study are available in the published article and its Supporting Information.

Supporting Information

The Supporting Information is available free of charge at https://pubs.acs.org/doi/10.1021/acs.joc.6c00674.

Experimental details, NMR spectra (^{1}H and $^{13}C\{^1H\}$) for all compounds, stability studies, ^{13}C-DEPT, IR spectroscopy, UV−vis spectroscopy, cyclic voltammetry, X-ray structures, and computational details (PDF)

Accession Codes

Deposition Numbers 2521891−2521895 contain the supporting crystallographic data for this paper. These data can be obtained free of charge via the joint Cambridge Crystallographic Data Centre (CCDC) and Fachinformationszentrum Karlsruhe Access Structures service.

■ AUTHOR INFORMATION

Corresponding Author

Tomas Marangoni − *Department of Chemistry, University of Maine, Orono, Maine 04469, United States; Frontier*

https://doi.org/10.1021/acs.joc.6c00674
J. Org. Chem. XXXX, XXX, XXX−XXX

Institute for Research in Sensor Technologies (FIRST), University of Maine, Orono, Maine 04469, United States; orcid.org/0000-0001-5825-7093;
Email: tomas.marangoni@maine.edu

Authors

Anjana Ranasinghe Meegasmullage − *Department of Chemistry, University of Maine, Orono, Maine 04469, United States*

Muhammad Usama Gul Khan − *Department of Chemistry, University of Houston, Houston, Texas 77204-5003, United States*

Jacob Mensah − *Department of Chemistry, University of Maine, Orono, Maine 04469, United States;* orcid.org/0000-0002-4735-6739

Sean Parkin − *Department of Chemistry, University of Kentucky, Lexington, Kentucky 40508, United States*

Alice E. Bruce − *Department of Chemistry, University of Maine, Orono, Maine 04469, United States;* orcid.org/0000-0002-4556-8180

Mitchell R. M. Bruce − *Department of Chemistry, University of Maine, Orono, Maine 04469, United States;* orcid.org/0000-0002-6428-3842

Judy I. Wu − *Department of Chemistry, University of Houston, Houston, Texas 77204-5003, United States;* orcid.org/0000-0003-0590-5290

Complete contact information is available at: https://pubs.acs.org/10.1021/acs.joc.6c00674

Author Contributions

The manuscript was written through contributions of all authors. All authors have given approval to the final version of the manuscript.

Notes

The authors declare no competing financial interest.

■ ACKNOWLEDGMENTS

T.M. thanks the National Science Foundation (NSF CHE-2511701) for support with the acquisition of the MALDI-TOF/TOF MS which was used for this manuscript. J.I.W. thanks the National Science Foundation (NSF CHE-2303851) for support. We acknowledge the use of the Carya and Sabine clusters and support from the Research Computing Data Core at the University of Houston. T.M. acknowledges the use of SEM at the UMaine CORE (Coordinated Operating Research Entities) and the help of Dr. Emma Perry. T.M. acknowledges Dr. Xiuli Mao (Mass Spectrometry Lab, University of Illinois Urbana—Champaign) for her help with mass spectrometry. T.M. thanks prof. Michael Haley for insightful discussions.

■ ABBREVIATIONS

TIPSA, triisopropylsilylacetylene; TIPS, triisopropylsilyl; TMSA, trimethylsilylacetylene; Ad-E, 1-ethynyladamantane; CV, cyclic voltammetry; NMR, nuclear magnetic resonance; IDT, indacenodithiophene; IF, indenofluorene; OFET, organic field effect transistors; OPV, organic photovoltaics; DFT, density functional theory; TD-DFT, time-dependent density functional theory; NICS, nucleus-independent chemical shift; NICS2BC, nucleus-independent chemical shifts to bond currents; ORTEP, Oak Ridge thermal ellipsoid plot program; HOMO, highest occupied molecular orbital; LUMO, lowest unoccupied molecular orbital; HR-MS, high-resolution mass spectrometry; ESI, electrospray ionization; EI, electron impact ionization

■ REFERENCES

(1) Merlet, S.; Birau, M.; Wang, Z. Y. Synthesis and Characterization of Highly Fluorescent Indenofluorenes. *Org. Lett.* **2002**, *4* (13), 2157−2159.
(2) Melidonie, J.; Liu, J.; Fu, Y.; Weigand, J. J.; Berger, R.; Feng, X. Pyrene-Fused s-Indacene. *J. Org. Chem.* **2018**, *83* (12), 6633−6639.
(3) Nishida, J.; Tsukaguchi, S.; Yamashita, Y. Synthesis, Crystal Structures, and Properties of 6,12-Diaryl-Substituted Indeno[1,2-b]Fluorenes. *Chem. - Eur. J.* **2012**, *18* (29), 8964−8970.
(4) Chase, D. T.; Rose, B. D.; McClintock, S. P.; Zakharov, L. N.; Haley, M. M. Indeno[1,2-b]Fluorenes: Fully Conjugated Antiaromatic Analogues of Acenes. *Angew. Chem., Int. Ed.* **2011**, *50* (5), 1127−1130.
(5) Frederickson, C. K.; Rose, B. D.; Haley, M. M. Explorations of the Indenofluorenes and Expanded Quinoidal Analogues. *Acc. Chem. Res.* **2017**, *50* (4), 977−987.
(6) Can, A.; Facchetti, A.; Usta, H. Indenofluorenes for Organic Optoelectronics: The Dance of Fused Five- and Six-Membered Rings Enabling Structural Versatility. *J. Mater. Chem. C* **2022**, *10* (22), 8496−8535.
(7) Chase, D. T.; Fix, A. G.; Rose, B. D.; Weber, C. D.; Nobusue, S.; Stockwell, C. E.; Zakharov, L. N.; Lonergan, M. C.; Haley, M. M. Electron-Accepting 6,12-Diethynylindeno[1,2-b]Fluorenes: Synthesis, Crystal Structures, and Photophysical Properties. *Angew. Chem.* **2011**, *123* (47), 11299−11302.
(8) Darvish, A.; Fernández, I.; Gagnon, F.; Morin, J.-F. Synthesis of Diindeno-Fused Dibenzochrysenes: A Route to Low-Bandgap Polycyclic Aromatic Hydrocarbons. *J. Org. Chem.* **2026**, *91* (3), 1264−1270.
(9) Saha, H. K.; Mallick, D.; Das, S. Dibenzoheterole-Fused s-Indacenes. *J. Org. Chem.* **2023**, *88* (23), 16248−16258.
(10) Barker, J. E.; Price, T. W.; Karas, L. J.; Kishi, R.; MacMillan, S. N.; Zakharov, L. N.; Gómez-García, C. J.; Wu, J. I.; Nakano, M.; Haley, M. M. A Tale of Two Isomers: Enhanced Antiaromaticity/Diradical Character versus Deleterious Ring-Opening of Benzofuran-Fused s-Indacenes and Dicyclopenta[b,g]Naphthalenes. *Angew. Chem., Int. Ed.* **2021**, *60* (41), 22385−22392.
(11) Saha, H. K.; Ghosh, S.; Mallick, D.; Senanayak, S. P.; Das, S. Dibenzo-Extended s-Indacenodicarbazole Isomers with Tunable Antiaromatic Characteristics: Impact of Aromaticity, Syntheses, and Properties. *J. Org. Chem.* **2025**, *90* (49), 17304−17313.
(12) Tra, B. Y. E.; Zhao, Y.; Molino, A.; Ouyang, Y.; Deng, C.-L.; McAloon, C.; McMillion, N. D.; Kim, H.; Zhang, C.; Müller, P.; Griffin, R. G.; Gilliard, R. J., Jr Diboron-Incorporated Indenofluorene: Isolation of Crystalline Neutral and Reduced States of 6,12-Diboraindeno[1,2-b]Fluorene. *J. Am. Chem. Soc.* **2025**, *147* (22), 18431−18437.
(13) Gul Khan, M. U.; Młodzikowska-Pieńko, K.; Gershoni-Poranne, R.; Wu, I. J. Three Wrongs Make a Right: A Computational Investigation of [4*n*]−[4*n*]−[4*n*] Fused π-Systems. *Chem. Sci.* **2026**, *17*, 8021−8027.
(14) Sahewal, S.; Ghosh, S.; Pradhan, P.; Sharma, P. K.; Saifuddin, M.; Patra, B. K.; Senanayak, S. P.; Das, S. S-Heterocyclic s-Indacenodifluorene: Synthesis, Properties, and Thermally Tunable Ambipolar Field-Effect Mobility. *Chem. - Eur. J.* **2025**, *31* (29), No. e202500725.
(15) Han, Y.; Zhu, J.; Dong, S.; Eng, Y.; Tao, T.; Gopalakrishna, T. Y.; Chi, C. Bisazapentalene Dication: Global Aromaticity and Open-Shell Singlet Ground State. *Org. Lett.* **2023**, *25* (19), 3380−3385.
(16) Saha, H. K.; Tarun; Mallick, D.; Pandey, U. K.; Das, S. N-Annulated Indenofluorene: An Isomeric Motif for N-Annulated Perylene. *Org. Lett.* **2025**, *27* (50), 13846−13851.
(17) Cummings, E.; Karadakov, P. B. Aromaticity in the Electronic Ground and Lowest Triplet States of Molecules with Fused Thiophene Rings. *Chem. - Eur. J.* **2024**, *30* (20), No. e202303724.

(18) Khelifi, W.; Luscombe, C. K. Recent Developments in Indacenodithiophene and Indacenodithienothiophene-Based Donor-Acceptor Conjugated Polymers: From Design to Device Performance in Organic Electronics. *Prog. Polym. Sci.* **2024**, *151*, No. 101804.
(19) Young, B. S.; Chase, D. T.; Marshall, J. L.; Vonnegut, C. L.; Zakharov, L. N.; Haley, M. M. Synthesis and Properties of Fully-Conjugated Indacenedithiophenes. *Chem. Sci.* **2014**, *5* (3), 1008−1014.
(20) Warren, G. I.; Barker, J. E.; Zakharov, L. N.; Haley, M. M. Enhancing the Antiaromaticity of S-Indacene through Naphthothiophene Fusion. *Org. Lett.* **2021**, *23* (13), 5012−5017.
(21) Jalife, S.; Wu, J. I. How Do Heteroatom Placements Affect the Paratropicities of Heteroaromatic-Fused Indacenes? *J. Org. Chem.* **2025**, *90* (11), 4012−4017.
(22) Frederickson, C. K.; Zakharov, L. N.; Haley, M. M. Modulating Paratropicity Strength in Diareno-Fused Antiaromatics. *J. Am. Chem. Soc.* **2016**, *138* (51), 16827−16838.
(23) Warren, G. I.; Zocchi, L. J.; Zakharov, L. N.; Haley, M. M. Comparison of Antiaromatic Properties in a Series of Structurally Isomeric Naphthothiophene-Fused s-Indacenes. *Chem. - Eur. J.* **2023**, *29* (40), No. e202301153.
(24) Warren, G. I.; Młodzikowska-Pieńko, K.; Jalife, S.; Demachkie, I. S.; Wu, J. I.; Haley, M. M.; Gershoni-Poranne, R. Effects of benzoheterocyclic annelation on the s-indacene core: a computational analysis. *Chem. Sci.* **2025**, *16*, 575−583.
(25) Vidal, E.; Warren, G. I.; Barker, J. E.; Haley, M. M. The Interplay of Antiaromaticity and Diradical Character in Diarenoindacenes and Diindenoarenes. *Chem. Sci.* **2025**, *16* (41), 19026−19047.
(26) Casares, R.; Martínez-Pinel, Á.; Rodríguez-González, S.; Márquez, I. R.; Lezama, L.; González, M. T.; Leary, E.; Blanco, V.; Fallaque, J. G.; Díaz, C.; Martín, F.; Cuerva, J. M.; Millán, A. Engineering the HOMO−LUMO Gap of Indeno[1,2-b]Fluorene. *J. Mater. Chem. C* **2022**, *10* (32), 11775−11782.
(27) Fu, X.; Zhao, D. Cyclo-Oligomerization of 6,12-Diethynyl Indeno[1,2-b]Fluorenes via Diradical Intermediates. *Org. Lett.* **2015**, *17* (22), 5694−5697.
(28) Hung, C.-E.; Lin, H.-C.; Ozawa, R.; Rout, Y.; Miyoshi, H.; Ie, Y.; Hisaki, I.; Cheng, Y.-J.; Tobe, Y. Taming m-Quionodimethanes by Dispersion Force: Cyclodimerization of (Trialkylsilyl)Ethynyl-Substituted Indeno[2,1-b]Fluorenes and Fluoreno[2,3-b]Fluorenes. *Chem. - Eur. J.* **2025**, *31* (54), No. e02053.
(29) Ren, L.; Liu, C.; Wang, Z.; Zhu, X. Isomeric Indacenedibenzothiophenes: Synthesis, Photoelectric Properties and Ambipolar Semiconductivity. *J. Mater. Chem. C* **2016**, *4* (23), 5202−5206.
(30) Lu, T.; Chen, F. Multiwfn: A multifunctional wavefunction analyzer. *J. Comput. Chem.* **2012**, *33* (5), 580−592.
(31) Kruszewski, J.; Krygowski, T. M. Definition of Aromaticity Basing on the Harmonic Oscillator Model. *Tetrahedron Lett.* **1972**, *13* (36), 3839−3842.
(32) Chen, Z.; Wannere, C. S.; Corminboeuf, C.; Puchta, R.; von Ragué Schleyer, P. Nucleus-Independent Chemical Shifts (NICS) as an Aromaticity Criterion. *Chem. Rev.* **2005**, *105* (10), 3842−3888.
(33) von Ragué Schleyer, P.; Maerker, C.; Dransfeld, A.; Jiao, H.; van Eikema Hommes, N. J. R. Nucleus-Independent Chemical Shifts: A Simple and Efficient Aromaticity Probe. *J. Am. Chem. Soc.* **1996**, *118* (26), 6317−6318.
(34) Paenurk, E.; Gershoni-Poranne, R. Simple and Efficient Visualization of Aromaticity: Bond Currents Calculated from NICS Values. *Phys. Chem. Chem. Phys.* **2022**, *24* (15), 8631−8644.

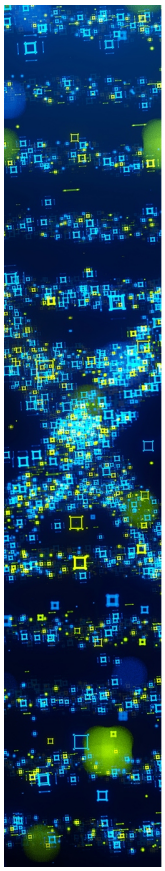
CAS BIOFINDER DISCOVERY PLATFORM™
STOP DIGGING THROUGH DATA —START MAKING DISCOVERIES
CAS BioFinder helps you find the right biological insights in seconds
Start your search
CAS
A division of the American Chemical Society

https://doi.org/10.1021/acs.joc.6c00674
J. Org. Chem. XXXX, XXX, XXX−XXX